Interactive oxidation of photoelectrocatalysis and electro-Fenton for azo dye degradation using TiO_2-Ti mesh and reticulated vitreous carbon electrodes

Y. B. Xie[a,b], X. Z. Li[a,*]

[a] *Department of Civil and Structural Engineering, The HongKong Polytechnic University, Hunghom, Kowloon, HongKong*

[b] *Key Laboratory of Molecular and Biomolecular Electronics, Southeast University, Nanjing 210096, China*

Abstract

A crystallized TiO_2 thin film was prepared by electrolytic anodization of a pure Ti mesh in sulfuric acid–phosphoric acid–hydrogen peroxide and hydrofluoric acid–sodium fluorid–hydrogen peroxide electrolyte solutions. The TiO_2 particles directly grown on the Ti mesh surface had the regular anatase crystal structure. The TiO_2 thin film showed a multiporous structure and the mean micropore size was about 260 nm. The azo dye orange-G degradation reaction was studied in an undivided cell by using the air-diffusion reticulated vitreous carbon as the cathode for the H_2O_2 electrogeneration and TiO_2-Ti mesh as the photoanode for the photoelectrocatalysis under ultraviolet light irradiation. The heterogeneous photoelectrocatalysis and the homogeneous electro-Fenton reaction simultaneously occurred in one reaction system, while H_2O_2 was produced by a two-electron reduction of oxygen and the ferrous ion was supplied by the dosing or electrogeneration method. In the photo-electro-integrated oxidation reaction system, both the degradation rate and the removal ratio of total organic carbon were enhanced for orange-G dye which was ascribed to interactive oxidation processes of photoelectrocatalysis, electro-Fenton and electrooxidation reaction. Ion chromatogram results indicate that the total mineralization reaction was much delayed to produce inorganic ions and groups although the complete decolorizing degradation could be achieved for orange-G dye.

Keywords: Anodization oxidation; Interactive oxidation; Photoelectrocatalysis; Titanium dioxide

[*] *Corresponding author: Tel: (852) 2766 6016; Fax: (852) 2334 6389; E-mail address: cexzli@polyu.edu.hk*

1. Introduction

In recent years, various technologies have been developed for environmental pollutants treatment [1,2]. Biological degradation was widely used for domestic wastewater treatment. However, many industrial organic pollutants are recalcitrant toward biological oxidation. Especially, this method is limited by the pollutants' toxicity to microorganisms or microorganisms' selectivity to various pollutants. Chemical oxidation may be a very effective method in most cases. However, this method becomes ineffective when pollutants are at low concentrations, or the chemical reagents may cause other environmental problems. At the same time, its operation cost is comparatively very high. Electrochemical oxidation (the use of electrical energy to drive a desired chemical reaction) and photochemical oxidation (the use of photon energy to drive a desired chemical reaction) are alternative technologies for environmental remediation.

Concerning the electrochemical oxidation technology, many investigations on the direct and indirect cathodic reduction and anodic oxidation of azoic dyestuffs demonstrate the suitability of these techniques for the decolorization and degradation of waste water from the textile dyeing industry [3,4]. Attractions of the electrochemical technology are the low cost of electricity compared with chemicals and the "green" issue of using only electrons as reagents. However, a significant drawback is that parasitic reactions, such as electrolysis of water, often compete with electrolysis of contaminants and its lower energy efficiency. Regarding the advanced oxidation technology of the semiconduction photocatalysis, titanium dioxide (TiO_2), due to its inexpensive, chemically stable, insoluble properties, has been proven to be an effective and suitable catalyst for non-selective oxidation and mineralization of various organic pollutants by photogenerated hydroxyl radicals in a mild condition. Many research works have been reported including the organic pollutant treatment of pesticides [5], dyes [6] and cyanides [7] wastewater. However, the TiO_2 photocatalytic reaction usually has a low rate of electron transfer to oxygen and a high rate of recombination between electron/hole pairs that result in a low quantum yield of < 5 % only. Therefore, photoelectrocatalytic oxidation becomes a good solution to further increase the efficiency by using electro-TiO_2-based photochemical oxidation systems.

In this study, the main idea was to realize both electrochemical oxidation and photocatalytic oxidation in one reaction system. A new process of H_2O_2-TiO_2 photoelectrochemical reaction has integrated the photocatalytic and electrolytic reaction for organic pollutants degradation [8]. A TiO_2-Ti mesh was used as photoanode to conduct the electro-assisted photocatalytic reaction, while a carbon electrode was used as cathode to generate H_2O_2 electrochemically. The photo-electro-assisted oxidation of the azo dye compound has been investigated. This reaction system has four advantages: (1) Avoiding the separation of the TiO_2 catalysts from the water phase by using photoelectrodes instead of free powder; (2) Restraining the recombination of electrons and holes by applying an electrical bias between TiO_2 anode and cathode; (3) Enhancing TiO_2 photocatalytic oxidation by electrochemical supply of H_2O_2 as a sacrificial oxidant to scavenge

conduction-band electron; (4) Further improving reaction efficiency by employing the interactive oxidation between electro-Fenton and photoelectrocatalysis. As a promising technology for pollutants degradation, the integrative advanced oxidation processes will offer the prospect of relatively higher efficiency than either photocatalytic oxidation or electrochemical oxidation alone [9,10].

2. Experimental details

2.1. Materials

The azo acid dye orange-G (OG) with chemical reagent grade was purchased from Sigma Chemical Co., and used without further purification. The molecule structure is shown in Fig. 1 and its ultraviolet (UV)-visible absorption spectrum is shown in Fig. 2.

[Fig. 1]

[Fig. 2]

Titanium dioxide powder (P25 TiO_2) with 80 % anatase and 20 % rutile was purchased from the Degussa AG Company and had an average particle size of 30 nm and a specific surface area of 50 m^2 g^{-1}. The inorganic reagents, such as $FeSO_4$, H_2SO_4, H_3PO_4, HF, NaF and H_2O_2, were analytical reagent grade quality and were purchased from Aldrich Chemical Co. Deionized and doubly-distilled water was used throughout this study. The electrode materials were TiO_2-Ti mesh, Pt sheet and reticulated vitreous carbon (RVC) foam. The Pt sheet was purchased from Sigma-Aldrich Co. Ltd. with 4.0 cm^2 area and 99.99 % purity. The titanium mesh (purity > 99.6 %, nominal aperture 0.19 mm, wire diameter 0.23 mm, wires/inch 60×60, open area 20 %, twill weave) was purchased from Goodfellow Cambridge Ltd. A duocel RVC foam (3 % nominal density, bulk density 1.54 g cm^{-3}, bulk resistivity 0.05 ohm·cm) was purchased from ERG Materials and Aerospace Corp. RVC is a new open pore foam material composed solely of vitreous carbon. RVC acts as porous cathode material for electrochemical processes that provides a large valid surface area and low electrical or fluid flow resistance, along with a great ability to hold infused materials within controlled porosity sizes. The surface morphology of the Ti mesh and RVC materials are shown in Fig. 3.

[Fig. 3]

2.2. Preparation of TiO_2-Ti mesh electrode

A TiO_2 thin film can be prepared on the surface of the Ti mesh by the electrochemical anodization method in a two-electrode electrolyzing system. Firstly, the raw titanium mesh (total area 5.0 cm^2) was washed with diluent HF acid and alcohol in a supersonic cleaner, then fully

rinsed with distilled water. This Ti mesh was carried out a controlled electrical oxidation process in the mixed acidic electrolyte solution by using a laboratory-made direct-current power supply (EPS 600, Electroophoresis Power Supply). The anodization process was conducted in two stages. In the first stage, the galvanostatic anodization with a constant current density of 60 mA cm^{-2} was performed in 100 ml of H_2SO_4 (1.5 M)－H_3PO_4 (0.3 M)－H_2O_2 (0.3 M) electrolyte solution until a designated anode-to-cathode voltage of 180 V was reached. This process lasted about 15 min. In the second stage, the potentiostatic anodization with a constant voltage of 180 V was maintained along with a gradual decrease of the current density until to 12 mA cm^{-2}. This anodization process also lasted about 15 min. Since three- or two-valence-state titanium ions were simultaneously produced in the bulk of the TiO_2 film during the anodization process, this TiO_2-Ti mesh was further electrolyzed in a NaF (0.03 M)－HF (0.03 M)－H_2O_2 (0.3 M) solution to removal the coexisting Ti^{2+}/Ti^{3+} ions by applying a constant electrode potential of 80 V and current density of 60 mA cm^{-2} for 5 min. Finally, the freshly generated TiO_2-Ti mesh electrode was rinsed by distilled water and dried in an oven at 105 °C for 4 h.

2.3. Photoelectrochemical reactor and experimental procedure

A schematic diagram of the batch-scale photoreactor system is shown in Fig. 4. It consists of a cylindrical silica glass reactor with an effective vessel volume of 80 ml, an external UV light source and a three-electrode configuration. As a photoanode, the TiO_2-Ti mesh was placed on the bottom of the reactor to receive UV light irradiation. The TiO_2 thin film supported on the Ti mesh was used as photocatalyst. As a cathode, a Pt or RVC sheet was placed nearby an air diffuser of the reactor. A saturated calomel electrode was used as a reference electrode. The electrode potential and working current were controlled with a ZF-9 potentiostat-galvanostat system. A medium-pressure mercury lamp was acted as UV light source (model LZC-UVA-365; power 8 W; average radiation intensity 0.68 mW cm^{-2}; main wavelength 365 nm). The photoelectrochemical experiments were performed with constant potential.

[Fig. 4]

To evaluate the reactivity of the electrochemical and photochemical oxidation reaction in the three-electrode system, several sets of degradation experiments were carried out in an undivided cell with the aerated aqueous solution. The electrochemical oxidation was established using the TiO_2-Ti mesh anode as a working electrode, the Pt sheet cathode as a counter electrode and a saturated calomel electrode (SCE) as a reference electrode under a dark condition. For the photoelectrocatalytic oxidation, UV light simultaneously irradiated to the TiO_2-Ti mesh for photocatalytic reaction on the base of the above electrochemical oxidation system. Additionally, an electro-Fenton reaction system was carried out in order to investigate the homogeneous

oxidation process for the OG dye degradation. A RVC cathode was applied for H_2O_2 electrogeneration, while Fe^{2+} was dosed into the OG solution prior to the reaction or continuously produced by anodization oxidation of the Fe sheet electrode during the whole process. The reaction solution was 30 ml azo dye OG with a concentration of 0.1 mM, pH= 6.2 and 0.01 M Na_2SO_4 supporting electrolyte. The air flow was controlled at 120 ml min^{-1} to supply the dissolved oxygen. The samples were collected from the reaction solution at regular intervals to determine the concentration by using a UV-visible spectrophotometer.

2.4. Analytical methods

To study the surface morphology, average pore size and pore distribution, scanning electron microscopy (SEM) (LEO Stereoscan 440) equipped with an energy-dispersive X-ray analysis facility (Oxford ISIS) was used. To determine the crystal phase composition of the prepared TiO_2 catalyst, X-ray diffraction (XRD) measurements were carried out on a Philips PW3020 diffractometer fitted with a graphite monochromator. An accelerating voltage of 40 kV and a current of 30 mA were used to produce Cu Kα radiation at a wavelength of 1.5418 Å. The samples were measured in the step scan mode with the step of 0.05 degree and a counting time of 1 s for angular range of $2\theta = 10-90°$. The absorption spectrum of the OG dye in aqueous solution was measured by a GENESYS 2 UV-visible spectrophotometer. The concentration was determined by the UV-visible absorption spectrum method and confirmed by the high-performance liquid chromatography method (HPLC) with an Atlantis reversed phase column (d-C18, 150 × 4.6 mm inner diameter, 5 μm beads); a mobile phase of acetonitrile/water = 70/30; flowrate of 1.0 ml min^{-1}; spectra system UV6000LP detector with a detecting wavelength of 480 nm; retention time of 3.12 min for the OG). The experimental results of two methods well agreed. The total organic carbon (TOC) concentration was measured by a Shimadzu TOC-5000A analyzer to determine the total mineralization degree of the OG compound during the advanced oxidation process. The total iron ion concentration was measured by a Perkin-Elmer 3300 atomic absorption spectrometer with a HGA-600 graphite furnace and auto sampler. Ion chromatography analysis was applied to determine the mineralization products of the OG degradation. The sulfate and nitrate ions were measured by the Shimadzu HIC-6A ion chromatography with a conductivity detector, in which a Shim-Pack IC-A1 anion column with a mobile phase containing 2.5 mM phthalic acid and 2.4 mM tris(hydroxymethyl)-aminomethane at a flow rate of 1.5 ml min^{-1}.

3. Results and discussion

3.1. Microstructure analyses

The morphology of the TiO_2-Ti mesh electrodes is shown in Fig. 5. Since the TiO_2 film was directly grown on the Ti mesh substrate, the TiO_2 particles could tightly adhered on the surface of the Ti mesh with a high physical strength. This TiO_2 film had a rough surface with a multiporous

microstructure. The mean micropore size was about 260 nm. During the anodic oxidation process in aqueous acidic solution, titanium metal can be oxidized into different valence ions (Ti^{2+}, Ti^{3+} and Ti^{4+}) when a higher positive potential was applied to the Ti mesh anode than its theoretical value vs. SCE (1.630 V for Ti^{2+}; 1.998 V for Ti^{3+}; 2.188 V for Ti^{4+}). Under the high potential electrolyzing condition, the main anodization product was the Ti^{4+} ion. Moreover, there is a competition process between the oxidation reaction of the Ti mesh electrode with the dissolved oxygen to form TiO_2 and the electrolytic dissolution reaction of TiO_2-Ti to form Ti^{4+} into aqueous solution. Practically, a much higher current density and cell potential were applied for a faster growing rate of oxide layer on the Ti mesh electrode. An earlier work about titanium mesh anodization indicated that the formation of micropores was ascribed to the power dissipation in the barrier oxide layer. When the anodizing current density was higher than 60 mA cm^{-2} in a H_2SO_4—H_3PO_4—H_2O_2 mixed solution, the thermal energy dissipation in the barrier oxide layer increased considerably. This current could cause a local overheating of the oxide, and the cooling of the oxidized anode by the electrolyte became insufficient. This local high temperature led to a high ionic current probably along the grain boundaries, which resulted in a porous surface [11]. So, the TiO_2 thin film could grow layer by layer on the Ti mesh surface and finally form a multiporous structure.

[Fig. 5]

3.2. XRD analysis of the TiO_2-Ti mesh electrode

[Fig. 6]

Fig. 6 shows the XRD patterns of TiO_2 thin films on the Ti mesh during the anodization process. The TiO_2 film prepared only by the galvanostatic anodization process mainly exhibited amorphous structure due to the weak scattering peak characteristic at $2\theta = 25.4^{\circ}$. Comparatively, after the galvanostatic and potentiostatical anodization process, the TiO_2 film could had formed the regular pure anatase crystal structure, which was ascribed to the appearance of diffraction peaks characteristic at $2\theta = 25.4^{\circ}$ for the (101) plane and $2\theta = 48.1^{\circ}$ for the (200) plane. This result means that the first galvanostatic anodization process mainly contributed to the Ti metal oxidation reaction to form amorphous TiO_2 and the subsequently potentiostatical anodization process led to recrystallize TiO_2 particles into the more regular anatase phase structure to achieve the complete crystallization. So, under this preparation condition, the anodization process could influence the degree of crystallization and structure of TiO_2 film [12].

3.3. Cyclic voltammetry analysis

In this study, the measurement of cyclic voltammogram was performed in a standard three-electrode assembly to investigate the electrochemical behaviour of electrodes. In the first experiments, while the Pt electrode acted as a working electrode in the OG solution, the RVC electrode acted as a working electrode in the oxygen saturated aqueous solution, respectively to study the OG electrochemical reaction and H_2O_2 electro-generation on individual electrodes. In both the experiments, a Pt electrode was used as a counter electrode and SCE as a reference electrode. The scanning rate was set at 20 mV s^{-1}.

The results of cyclic voltammogram of Pt-Pt and RVC-Pt electrodes are shown in Fig. 7, respectively. Fig. 7a shows that only one pair of current peak appeared in the cyclic voltammogram which was ascribed to the reversible redox reaction at -0.282 V for the cathode reduction and at 0.415 V for the anode oxidation process in the OG solution. Its corresponding current intensity involved 0.249 mA for the anodic current peak and -0.308 mA for the cathode current peak. This voltammetric profile does not undergo significant changes when the working potential cycled for several times between 1.25 V and -1.25 V at the scanning rate of 20 mV s^{-1}. The potential distance from the anodic current peak potential E_{pa} to the cathodic current peak potential E_{pc} was defined as ($E_{pa} - E_{pc}$), whose calculated value was 0.697 V. Similarly, the ratio of the corresponding peak currents was defined as (I_{pc}/I_{pa}), whose calculated value was 0.808. This result ($I_{pc}/I_{pa} < 1.0$) means that the reversible redox reaction of the OG dye was a typical multi-electron transfer process [13]. The existence of an oxidation peak and a reduction peak means that the OG dye could carry out the decolorizing degradation reaction either by a direct electroreduction or electrooxidation process. Fig. 7b shows that the critical reduction potential was -0.495 V on the RVC electrode for the H_2O_2 generation in an oxygen-saturated solution. So, in this study, the RVC cathodic bias potential of -0.71 V was high enough for the H_2O_2 generation during the electro-reduction process which was helpful to promote the H_2O_2-TiO_2 synergetic oxidation and electro-Fenton reaction.

[Fig. 7]

As a function electrode, the TiO_2-Ti anode could carry out various electrochemical reactions during the OG degradation. In the following two experiments, the TiO_2-Ti mesh electrode acted as a working electrode, the Pt electrode as a counter electrode and the SCE as a reference electrode. The cyclic voltammogram experiments were performed in Na_2SO_4 solution with and without the OG. The results are shown in Fig. 8. It can be seen that the oxidation potential was 1.825 V vs. SCE for $2H_2O - 4e^- \rightarrow O_2 + 4H^+$ on the TiO_2-Ti mesh electrode (see Fig. 8a). According to its standard potential of 1.229 V vs. NHE (normal hydrogen electrode), the overpotential was 0.355 V for oxygen generation on the TiO_2-Ti mesh electrode. Actually, the TiO_2-Ti mesh working potential was only employed to 0.71 V in this study, which is significantly lower than 1.825 V. So,

the oxygen generation on the TiO_2-Ti electrode surface has been minimized. An important consideration is that the electrochemical reaction often occurs at low electrode potentials to avoid the corrosion of TiO_2 catalyst. Therefore, the parasitic electrolysis of water could be neglected on this experimental condition. Additionally, the oxidation peak in the cyclic voltammogram curve means that the OG molecule could be directly oxidized on the TiO_2-Ti electrode surface when the anode potential was higher than 0.588 V (see Fig. 8b).

[Fig. 8]

3.4. Degradation reaction

The three-dimensional multipore electrodes, including TiO_2-Ti mesh and RVC, could effectively adsorb organic dye molecules on the interface. Prior to photoelectrochemical reaction, the dark adsorption-desorption equilibrium experiment was achieved under oxygen-free condition. The concentration decreased from 0.100 to 0.089 mM for a new TiO_2-Ti/RVC electrode pair and to 0.099 mM for a new TiO_2-Ti/Pt electrode pair. The RVC electrode shows a better interfacial adsorption effect on the OG dye, which is due to its high special surface area of 65 cm^2 cm^{-3}. Therefore, in order to remove the influence of physical adsorption in deferent reaction systems, all electrodes were immersed in the OG solution for 2 h to reach saturation adsorption before the degradation reaction.

3.4.1 Photochemical oxidation

The photochemical oxidation process includes direct photolytic and photocatalytic oxidation degradation under UV light irradiation, which contributes to the decomposition reaction of the dye molecule. Fig. 9 shows that the OG dye concentration decreased from 0.100 to 0.099 mM for only UV direct photolysis and to 0.928 mM for UV photocatalysis of the TiO_2-Ti mesh. The total degradation ratio of the OG dye was 1.0 % for photolysis and 7.2 % for photocatalysis after 300 min. The corresponding TOC values also decreased from initial 12.63 to final 12.02 and 11.08 mg l^{-1}, respectively.

[Fig. 9]

The organic dye could be oxidized by the first excited singlet oxygen ($^1O_2{}^*(S_1)$), which was generated from the ground state oxygen ($^3O_2$) by absorbing UV light photon energy ($h\upsilon$) emitted from the first excited triplet state of dye molecule ($^3Dye^*(T_1)$).

$$^3O_2 \xrightarrow[\text{dye}]{h\upsilon} {}^1O_2{}^* \qquad \text{dye} + {}^1O_2{}^* \longrightarrow \text{degradation products}$$

However, this process could be neglected due to its very low reaction efficiency. Comparatively, TiO_2 photocatalysis involved the hydroxyl radicals' oxidation reaction with the OG on the catalyst surface. Hydroxyl radicals were generated from the photogenerated holes by electrons excitation and transfer under UV light irradiation.

$TiO_2 + h\upsilon \rightarrow e^- + h^+$

$e^- + O_2 \rightarrow O_2^{-\cdot}$

$O_2^{-\cdot} + H^+ \rightarrow HOO\cdot$; $2\ HOO\cdot \rightarrow H_2O_2 + O_2$; $H_2O_2 + O_2^{-\cdot} \rightarrow \cdot OH + OH^- + O_2$

$h^+ + H_2O \rightarrow \cdot OH + H^+$

dye + $\cdot OH$ (or h^+) $\rightarrow$ degradation products

In comparison with photolysis, the decolorizing degradation ratio has apparently improved by the phototcatalysis process. This experimental result indicates that neither the electrooxidation nor photocatalytic oxidation process is an effective method for the OG dye complete degradation due to the low electrolyzing efficiency for electrooxidation and low e^-—h^+ pair separation efficiency for the heterogeneous photocatalysis. When a certain anodic bias potential was applied to the TiO_2-Ti photoanode, the photocatalytic reaction system could be modified into a photoelectrocatalytic reaction system. After 300 min, the OG concentration decreased from 0.1 to 0.075 mM and the TOC value decreased from initial 12.63 to 9.25 mg l^{-1}. So, both the total degradation ratio and TOC removal ratio were obviously improved in the electro-assisted photocatalysis process. Its degradation efficiency was even higher than the sum of the individual electrooxidation and photocatalysis processes.

3.4.2. Electrochemical oxidation

Regarding the redox peaks in the cyclic voltammetry, the OG dye can be directly degraded by electrolytic oxidation process in aqueous solution when the anode bias potential was applied above its critical potential. So, an electrochemical oxidation process was carried out to investigate the degradation effect of the OG dye.

3.4.2.1. Anode electrooxidation

The anode electrooxidation process involves organic compound degradation by the electrochemical reaction on the anode surface. Electron transfer from the dye molecule to the anode could cause the direct oxidation of the OG dye by an electrolysis process when the anode potential was higher than 0.588 V. Additionally, hydroxyl radicals also could participate in the oxidation reaction of the OG dye, which was generated from the electrolytic oxidation of water on the anode surface when the electrode potential was higher than 1.776 V [14,15]. In this study, the production of hydroxyl radicals via the oxidation of $H_2O - e^- \rightarrow \cdot OH + H^+$ could be neglected due to the low applying electrolytic potential of 0.71 V. Actually, the OG dye could diffuse to the

surface of the TiO_2-Ti electrode where it underwent the electrons transfer. This process contributes to the formation of anodic current and the short-lived dye cation radical ($dye^{+\cdot}$). The $dye^{+\cdot}$ intermediate was very unstable and active which could be oxidized with reactive oxygen molecules by the reaction of $dye^{+\cdot} + O_2 \rightarrow$ degradation products. The $dye^{+\cdot}$ formation was assumed to be the slowest step in the whole degradation process. Regarding the electrooxidation of the OG dye, the TiO_2-Ti mesh working electrode was controlled at 0.71 V as a fixed anodic bias potential. The Pt sheet counter electrode acted as cathode. The pH value of the original OG dye solution was about 6.2 and it was not further adjusted. The initial working current of the electrolytic reaction was about 0.048 mA and the reaction cell potential was 0.85 V. The time-dependent OG degradation by direct electrolyzing oxidation is summarized in Fig. 9. It was noted that the total OG degradation ratio only achieved to 3.4 % after 300 min. So, the OG degradation efficiency was very low during the electrolytic oxidation process due to the very low working current under this condition.

3.4.2.2. Electro-Fenton oxidation

The electro-Fenton oxidation process involves the electrolytic generation of H_2O_2 together with ferrous ions to conduct the Fenton reaction for the organic compound degradation in a homogeneous system [16,17]. H_2O_2 is produced by the two-electron reduction of O_2 on various O_2-diffusion carbon cathodes by the reaction of $O_2 + 2H^+ + 2e^- \rightarrow H_2O_2$. By dosing ferrous ions into the acidic OG aqueous solution or by electrogeneration ferrous ions from Fe electrode anodization, the classical Fenton reaction can be established in the above system by the reaction of $Fe^{2+} + H_2O_2 \rightarrow Fe^{3+} + \cdot OH + OH^-$. UV light illumination would favor the production of hydroxyl radicals by the reaction of $H_2O_2 + h\upsilon \rightarrow 2\cdot OH$ and $Fe^{2+} + H_2O_2 + h\upsilon \rightarrow Fe(OH)^{2+} + \cdot OH$. Fe^{2+} regeneration was also promoted by the reaction of $Fe(OH)^{2+} + h\upsilon \rightarrow Fe^{2+} + \cdot OH$. Finally, the OG dye was degraded by the reaction of dye + $\cdot OH \rightarrow$ degradation products.

[Fig. 10]

For the photo-assisted electro-Fenton reaction, the RVC working electrode was controlled at -0.71 V as the cathode bias potential. The pH value of the OG solution was adjusted to 3.0 with hydrochloric acid. The total iron ion concentration was 17.8 mg l^{-1} in the OG solution by the chemical dosing method. The initial cathodic current was about -12 mA in degradation reaction. Fig. 10 shows the characteristic absorption peaks of the azo structure and naphthalene ring structure have decreased sharply and almost disappeared completely after 300 min. The OG degradation ratio has reached to about 76.6 % after 60 min and to about 100 % after 300 min. The TOC value decreased from 12.6 to 6.1 mg l^{-1} after 300 min. Therefore, the photo-assisted electro-Fenton system was very effective for the OG degradation. It also can been see from the

inserted graph that a linear-fit relationship between ln(C_0/C) and irradiation time t was obtained, which means the OG dye degradation follows a pseudo-first-order kinetics with an apparent first-order constant of 0.0182 min^{-1}.

3.4.3. Electro-assisted photocatalytic oxidation

The electro-assisted photocatalytic oxidation process involves the photocatalytic oxidation reaction on the TiO_2 electrode to which a certain anode bias potential was applied in order to remove the photogenerated electrons for promoting the separation efficiency of the electro-hole pair [18]. This photoelectrocatalytic oxidation reaction was conducted on the TiO_2-Ti mesh anode surface under UV light irradiation [19, 20].

Step 1: $TiO_2 + h\upsilon \rightarrow e^- + h^+ \rightarrow e^-$ (electron transfer by out-electrocircuit) + h^+

Step 2: $h^+ + H_2O$ (or OH^-) $\rightarrow$ ·OH and dye + ·OH (or h^+) $\rightarrow$ degradation products

In the first step, by applying an anodic bias potential to the TiO_2-Ti mesh working electrode, a potential gradient was provided within the TiO_2 photocatalyst film to efficiently force the electrons to arrive at the counter electrode, and the left photogeneration holes would react with H_2O/OH^- to give rise of hydroxyl radicals. In the second step, the photogenerated holes and hydroxyl radicals can effectively conduct the oxidation reaction for the OG dye degradation.

[Fig. 11]

In this study, the role of H_2O_2 was investigated in the photoelectrocatalytic process. A TiO_2-Ti mesh was the working electrode and its anodic bias potential was controlled at 0.71 V. When Pt was used as cathode, the initial working cell current was 0.028 mA and the corresponding Pt cathode potential was -0.242 V. It would be unlikely to conduct H_2O_2 generation on the surface of the Pt electrode under this condition. However, when RVC was used as a cathode, the initial working cell current was 0.048 mA and the corresponding cathode potential was -0.540 V, which was available enough for H_2O_2 generation on the RVC electrode. The degradation efficiency was 49.9 % for the TiO_2-Ti /RVC electrode system and 25.1 % for the TiO_2-Ti/Pt electrode system after 300 min (see Fig. 11). So, the electrogeneration of H_2O_2 on the RVC cathode could greatly promote the reaction activity of the TiO_2 catalyst. The H_2O_2-assisted TiO_2 photoelectrocatalytic oxidation process demonstrated higher decolorizing degradation efficiency than the sole photoelectrocatalysis. Moreover, its total degradation efficiency was even higher than the sum of the individual processes of photocatalysis (7.2 %), electrooxidation (3.4 %) and electro-assisted photocatalysis (25.1 %). This result was mainly ascribed to the H_2O_2-TiO_2 synergetic oxidation effect. The electrogeneration of H_2O_2 could assist the TiO_2 photoelectrocatalytic reaction to further promote the hydroxyl radicals production under UV light irradiation

$TiO_2 + h\upsilon \rightarrow TiO_2(h^+ + e^-)$

$O_2 + e^- \rightarrow O_2^-$ or electron transfer by out-electrocircuit

$H_2O(ads) + h^+ \rightarrow \cdot OH + H^+$

$OH^-(ads) + h^+ \rightarrow \cdot OH$

$H_2O_2 + h\upsilon \rightarrow 2\cdot OH$

$H_2O_2 + O_2^- \rightarrow \cdot OH + OH^- + O_2$

$H_2O_2(ads) + e^- \rightarrow \cdot OH + OH^-$

However, at high concentration of H_2O_2, the following reactions may predominate which restrained the degradation rate due to the self-consumption of hydroxyl radicals.

$H_2O_2 + HO\cdot \rightarrow H_2O + HOO\cdot$

$HOO\cdot + HO\cdot \rightarrow H_2O + O_2$

The H_2O_2 production by the continuous electrogeneration method could be controlled by current or potential adjusting. Therefore, this method was more feasible than the chemical dosing method, since an overdosing of H_2O_2 could be inhibitive to the photocatalytic oxidation reaction.

3.4.4. Electro-Fenton photoelectrocatalytic oxidation

The electro-Fenton photoelectrocatalytic oxidation process involved the heterogeneous photoelectrocatalytic reaction of TiO_2 and the homogeneous electro-Fenton reaction to take place simultaneously in one system [21]. In the RVC/TiO_2-Ti electrode pair system, the Fenton reaction was established by introducing the electrogeneration H_2O_2 on the O_2-diffusion RVC cathode and externally dosing Fe^{2+} in a certain acidic solution [22]. Meanwhile, the photoelectrocatalytic reaction occurred on the TiO_2 surface by applying the anode bias potential on the TiO_2-Ti mesh electrode. Regarding the electro-Fenton reaction, the ferrous iron was easily oxidized into ferric iron. Fe^{2+} regeneration could occur by the reactions of $Fe^{3+} + H_2O_2 \rightarrow Fe^{2+} + H^+ + HOO\cdot$, $Fe^{3+} + HOO\cdot \rightarrow Fe^{2+} + H^+ + O_2$, and $Fe(OH)^{2+} + h\upsilon \rightarrow Fe^{2+} + H^+ + HO\cdot$.

Two sets of the OG degradation experiments were carried out to investigate the electro-Fenton photoelectrocatalytic oxidation process. The first system adopted a RVC/TiO_2-Ti electrode pair with the external ferrous ion. The RVC working electrode was controlled at -0.71 V as cathode bias potential. The pH value was adjusted to 3.0 with hydrochloric acid. The initial working current was -11.47 mA. The initial ferrous ion concentration was 17.24 mg l^{-1} in the OG solution by the externally dosing method. The experimental result is shown in Fig. 12. The characteristic absorption peaks of the azo structure and naphthalene ring structure have completely disappeared and the absorption peak of the benzene ring structure has obviously decreased after 300 min. The total degradation ratio of the OG was 83.0 % after 60 min. The TOC value decreased to 3.31 mg l^{-1} after 300 min. The linear-fit relationship between $\ln(C_0/C)$ and irradiation time t was also obtained. So, the OG dye degradation followed a pseudo-first-order kinetics with an apparent first-order constant of 0.0194 min^{-1}. In comparison with the above electro-Fenton system, the electro-Fenton photoelectrocatalysis system did not have an obvious improvement of the OG degradation

efficiency. However, this reaction system was very effective for the TOC removal effect. Thereby, as a homogeneous reaction, the electro-Fenton reaction must have played a key role for the OG degradation. The TiO_2 photocatalytic and photoelectrocatalytic reaction could promote the mineralization of the OG degradation products. The working current, which was greatly dependent on the ferrous ion concentration, supporting the electrolyte concentration and pH value, played a very important role to determine the H_2O_2 generation efficiency when the RVC cathode bias potential was controlled at a more negative value than the critical potential value.

[Fig. 12]

The second system adopted a RVC/TiO_2-Fe electrode pair. A TiO_2 thin film was coated on the surface of the stainless-steel sheet by using the dip-coating method in 1.0 wt.% P25 TiO_2 aqueous suspension and subsequent heat treatment at 200 ºC for 2 h. This composite electrode of the stainless-steel sheet with TiO_2 coating film was denoted as TiO_2-Fe anode. The RVC working electrode was controlled at -0.71 V as cathode bias potential. The other experimental condition was the same as above except for the anodic material. So, the electrooxidation of the Fe sheet itself and the electroreduction of O_2 on the RVC electrode occurred simultaneously, which contributed to the continuous electrogeneration of Fenton's reagent. The initial working current was -1.72 mA and the total iron ion concentration by electrolytic generation was 16.72 mg l^{-1} after 300 min. Fig. 13 shows that the total degradation ratio reached to 56.5 % after 60 min. The TOC value decreased from 12.63 to 7.18 mg l^{-1} after 300 min. But the OG dye degradation reaction did not follow the pseudo-first-order kinetics due to the non-linear relationship between $\ln(C_0/C)$ and irradiation time t (see the inserted graph of Fig. 13).

[Fig. 13]

3.4.5. Photo-electro-assisted advanced oxidation

The OG molecular has an azo chromophoric group with Π-conjugation structure. One azo moiety has a naphthalene ring with an electron-donating –OH group and two electron-withdrawing $–SO_3Na$ groups. Another azo moiety is an attached benzene ring. The decomposition of the azo group and naphthalene ring, which was corresponding to the characteristic absorption at 478 and 330 nm respectively, was studied and compared during photo-electro-assisted interactive oxidation process as shown in Fig. 14. Regarding the OG degradation at λ=478 nm, the total decolorizing degradation has completely achieved after 300 min for all photo-electro-assisted oxidation processes (see Fig. 14a). However, concerning the OG degradation at λ=330 nm after 300 min, the naphthalene degradation ratio was 92.5 % for the photo-assisted electro-Fenton, 96.8 % for the electro-Fenton photoelectrocatalysis of the RVC/TiO_2-Ti electrodes by the dosing Fe^{2+}

and 72.7 % for the electro-Fenton photoelectrocatalysis of RVC/TiO_2-Fe electrodes by the electrogeneration Fe^{2+} (see Fig. 14b).

This result shows that the decomposition of the azo chromophoric group was more effective than that of the naphthalene ring structure in the above advanced oxidation processes. So, the predominant oxidation reaction of the OG molecule usually occurred on azo groups to destroy its molecule Π-conjugation structure which mostly caused the decolorizing degradation effect. Regarding the ferrous ion applied in the above advanced oxidation processes, it triggered the Fenton reaction to cause a very effective degradation of the OG dye. Moreover, it did not lead to an obvious difference in the decolorizing degradation efficiency between the externally dosing and electrogeneration method for ferrous ion. Comparatively, the TOC removal ratio was further improved by using the dosing method which was due to its higher current efficiency for the electrochemical process in the OG solution. However, it should be noted that the electrogeneration ferrous iron could be very easily realized by the parallel electrolyzing reaction in the same reaction system. So, it still can be regarded as a substituted method in the photo-electro-assisted advanced oxidation process. For all electro-Fenton reaction systems, H_2O_2 can be continuously produced by electrochemical method and its generation rate can be easily controlled by adjusting the working potential or current. Additionally, electrogeneration of H_2O_2 was a very effective supply method for the above synergetic oxidation reaction.

[Fig. 14]

The results of the TOC removal ratio show that OG dye could not be completely degraded and mineralized into CO_2, H_2O, inorganic ions and groups either by photochemical or electrochemical oxidation. Comparatively, the mineralization efficiency was obviously improved in the integrative photo-electro-assisted advanced oxidation processes. In fact, the OG dye was firstly degraded into sulfonic, nitro and nitroso compounds as intermediates, and then gradually oxidized into inorganic ions or groups. The characteristic mineralization products, sulfate ion and nitrate ion concentration could be determined by ion chromatography analysis. The theoretical values were calculated as 27.16 mg l^{-1} for the sulfate ion and 7.68 mg l^{-1} for the nitrate ion after complete mineralization of 0.1 mM OG. The mineralization ion concentrations were measured after 300 min in the above photo-electro-assisted advanced oxidation processes as shown in Fig. 15.

[Fig. 15]

Fig. 15 shows the mineralization degree of the nitro/nitroso group was more effective than the sulfonic group which was due to the predominant oxidation of the azo group for the OG

degradation. It also demonstrated a weak mineralization effect for the electro-Fenton photoelectrocatalysis process of the RVC/TiO_2-Fe electrodes. However, the electro-Fenton photoelectrocatalysis of the RVC/TiO_2-Ti electrodes exhibits the highest mineralization efficiency. The interactive oxidation reaction between the Fenton reaction and photoelectrocatalysis must have played a key role since H_2O_2 not only acted as the Fenton reagent but also promoted the photoelectrocatalytic reaction. Thereby, the homogeneous Fenton reaction and the heterogeneous photoelectrocatalytic reaction could occur simultaneously in one system and the individual oxidation reaction was promoted by each other. The H_2O_2 generation on the RVC electrode greatly depended on the working current efficiency which was determined by the supporting electrolyte strength and working circuit resistance. As a result, the mineralization efficiency for sulfate and nitrate ions obviously improved under high current density by the interactive oxidation of the photoelectrocatalysis and the electro-Fenton reaction in one reaction system.

4. Conclusions

A novel H_2O_2-TiO_2 photoreactor system was specially designed to realize both the electrochemical and photocatalytic oxidation in an undivided reaction cell, which was equipped with an ultraviolet light source and two functional electrodes by using an anodization TiO_2-Ti mesh as a photoanode and a high special area RVC as a cathode. The electro-Fenton photoelectrocatalysis reaction was also realized by using RVC and composite TiO_2-Fe as electrodes for a simultaneous electrogeneration of H_2O_2 and ferrous ions. Orange-G dye was effectively degraded by interactive oxidation of a heterogeneous photoelectrocatalysis and a homogeneous Fenton oxidation reaction in one system. The synergetic effect contributed to the high reactivity of the TiO_2 photoelectrocatalytic reaction by continuously introducing H_2O_2 through the electrolytic method. It may provide a new approach for further development of photo-electro-assisted oxidation reactions for organic pollutants degradation in the future.

Acknowledgement

This work was financially supported by The Research Grants Council of Hong Kong (Grant No. PolyU5148/03E).

References

[1] E. Kusvuran, O. Gulnaz, S. Irmak, O.M. Atanur, H.I. Yavuz, O. Erbatur, J. Hazardous Mater. B 109 (2004) 85.

[2] E. Brillas, J.C. Calpe1, J. Casado, Wat. Res. 34 (2000) 2253.

[3] A. Roessler, D. Crettenand, Dyes Pigments 63 (2004) 29.

[4] J.P. Lorimer, T.J. Mason, M. Plattes, S.S. Phull, D.J. Walton, Pure Appl. Chem. 73 (2001) 1957.

[5] S. Malato, J. Blanco, J. Cáceres, A.R. Fernández-Alba, A. Agüera, A. Rodriguez, Catal. Today 76 (2002) 209.

[6] K. Tanaka, K. Padermpole, T. Hisanaga, Wat. Res. 34 (2000) 327.
[7] K. Chiang, R. Amal, T. Tran, J. Mol. Catal. A: Chem. 193 (2003) 285.
[8] E. Brillas, M.A. Bannos, S. Camps, C. Arias, P.L. Cabot, J.A. Garrido, R.M. Rodriguez, New J. Chem. 28 (2004) 314.
[9] M. Pera-Titus, V. Garcia-Molina, M.A. Baños, J. Giménez, S. Esplugas, Appl. Catal. B: Environ. 47 (2004) 219.
[10] F. Shiraishi, T. Nakasako, Z.Z. Hua, J. Phys. Chem. A 107 (2003) 11072.
[11] R.W. Matthews, Wat. Res. 24 (1990) 653.
[12] B. Karunagaran, R.T.R. Kumar, D. Mangalaraj, S.A.K. Narayandass, G. Mohan Rao, Cryst. Res. Technol. 37 (2002) 1285.
[13] S.R. Biaggio, N. Bocchi , R.C. Rocha-Filho, F.E. Varela, J. Braz. Chem. Soc. 8 (1997) 615.
[14] E. Fockedey, A. Van Lierde, Wat. Res. 36 (2002) 4169.
[15] G. Chen, E.A. Betterton, R.G. Arnold, J. Appl. Electrochem. 29 (1999) 961.
[16] A. Ventura, G. Jacquet, A. Bermond, V. Camel, Wat. Res. 36 (2002) 3517.
[17] M.A. Oturan, N. Oturan, C. Lahitte, S. Trevin, J. Electroanal. Chem. 507 (2001) 96.
[18] H. Selcuk, W. Zaltner, J.J. Sene, M. Bekbolet, M.A. Anderson, J. Appl. Electrochem. 34 (2004) 653.
[19] G. Waldner, M. Pourmodjib, R. Bauer, M. Neumann-Spallart, Chemosphere 50 (2003) 989.
[20] M.V.B. Zanoni, J.J. Sene, M.A. Anderson, J. Photochem. Photobiol. A: Chem. 157 (2003) 55.
[21] S.R. Kanel, B. Neppolian, H. Choi, J.W. Yang, Soil Sed. Contam. 12 (2003) 101.
[22] B. Boye, M.M. Dieng, E. Brillas, J. Electroanal. Chem. 557 (2003) 135.

List of figure captions

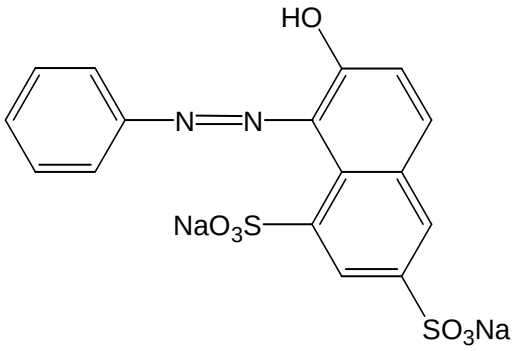

Fig. 1. The molecule structure of dye orange-G (chemical formula = $C_{16}H_{10}N_2O_7S_2Na_2$, formula weight = 452.386).

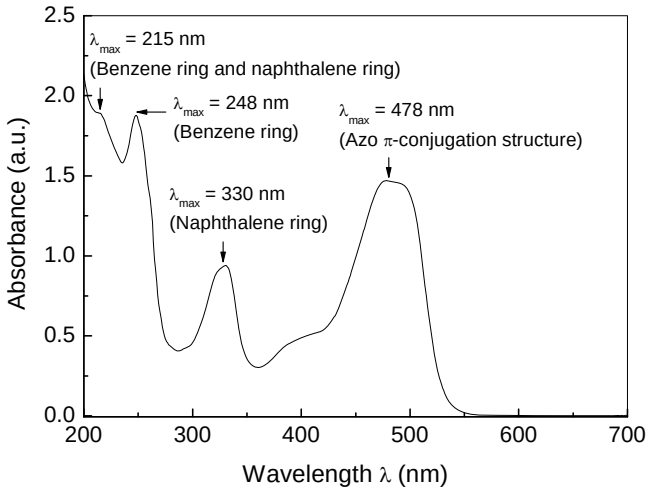

Fig. 2. UV-visible absorption spectrum of 0.1 mM OG dye in aqueous solution.

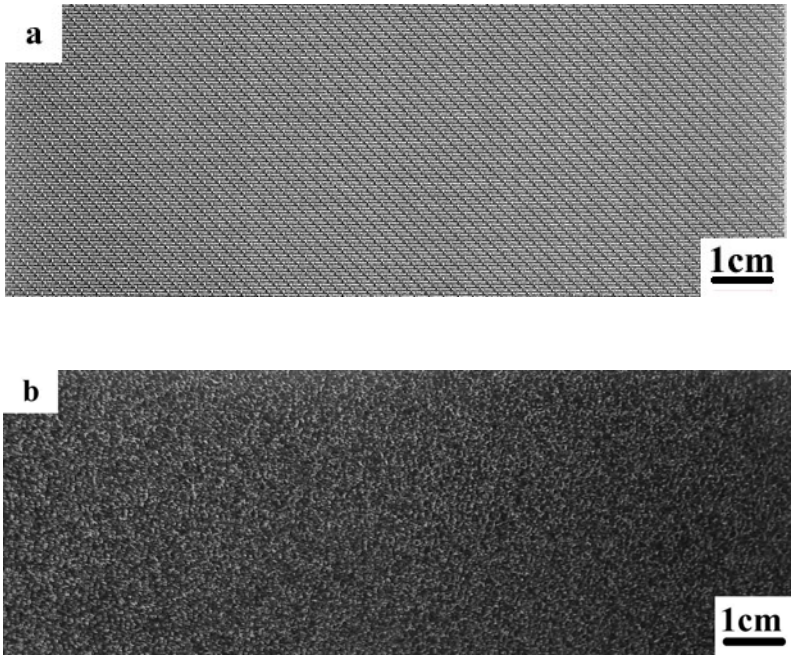

Fig. 3. SEM images of (a) the raw titanium mesh and (b) RVC electrode material.

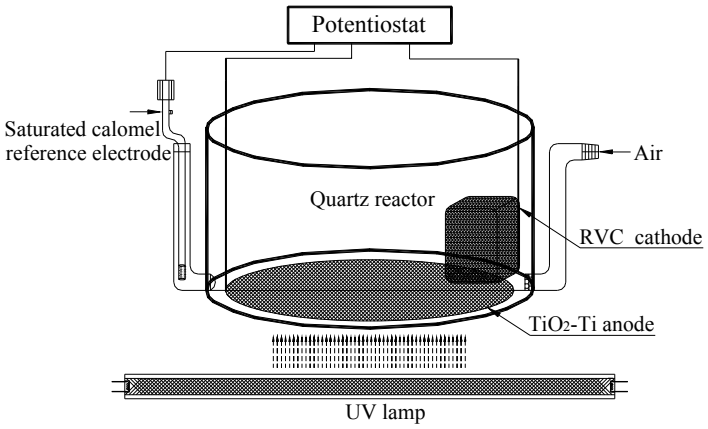

Fig. 4. Schematic diagram of the photoreaction equipment with an UV light source.

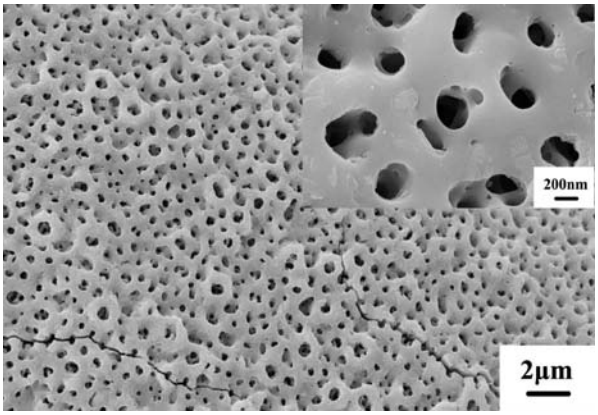

Fig. 5. SEM images of TiO_2 thin film using the anodization treatment from the Ti mesh.

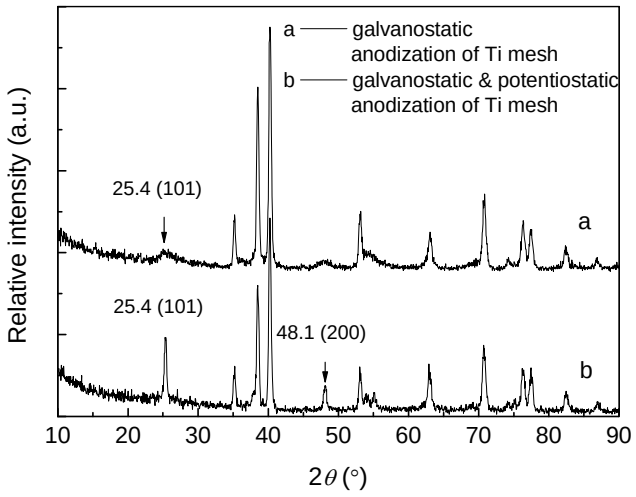

Fig. 6. XRD pattern of the TiO_2 thin film using the anodization method from the Ti mesh.

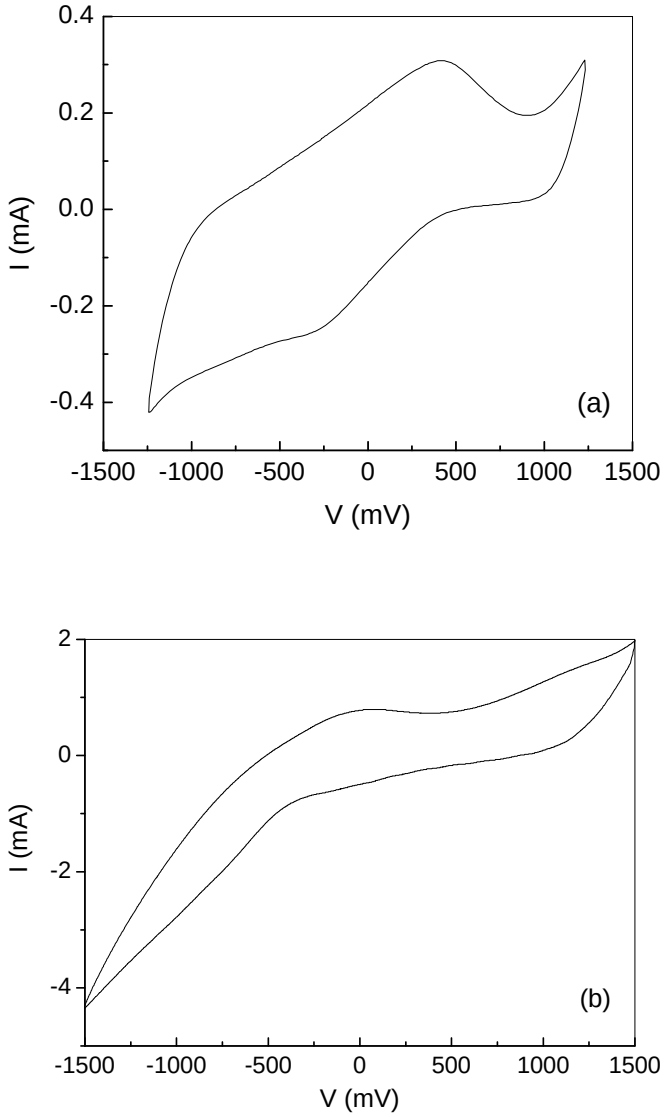

Fig. 7. Cyclic voltammogram of a (a) Pt electrode in 0.1 mM OG aqueous solution with 0.01 M Na_2SO_4 and (b) RVC electrode in oxygen-saturated aqueous solution with 0.01 M Na_2SO_4.

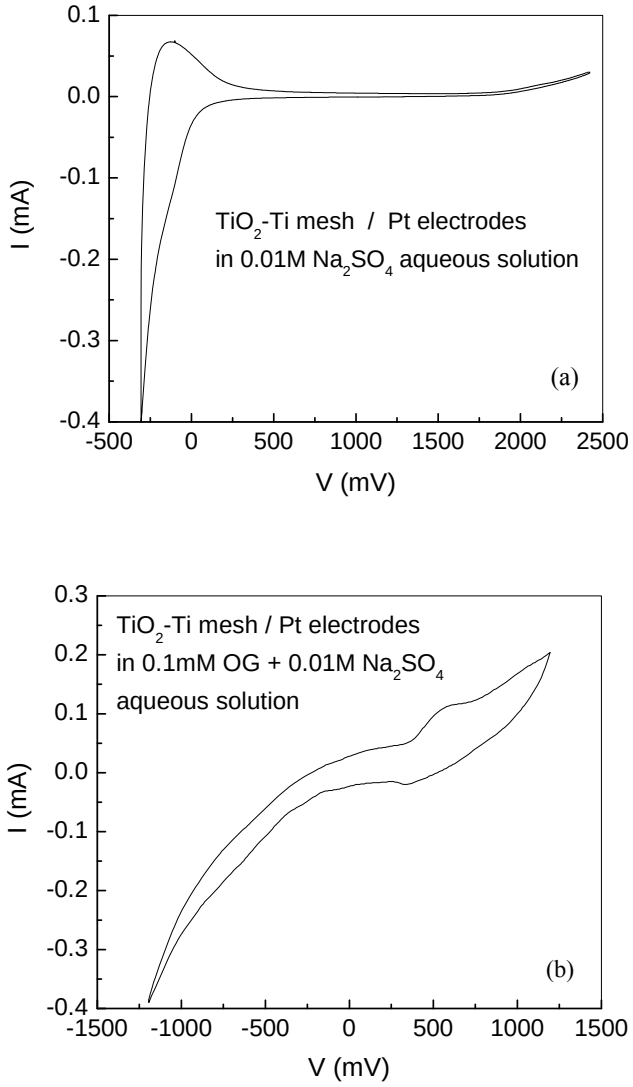

Fig. 8. Cyclic voltammogram of the TiO_2-Ti mesh electrode in (a) 0.01 M Na_2SO_4 aqueous solution and (b) 0.1 mM OG + 0.01 M Na_2SO_4 aqueous solution.

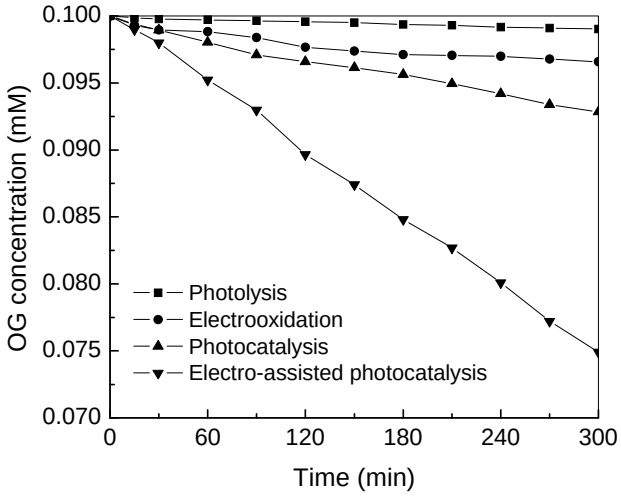

Fig. 9. Decrease of the OG concentration during photolysis, electrooxidation, photocatalysis and electro-assisted photocatalysis processes under UV light irradiation.

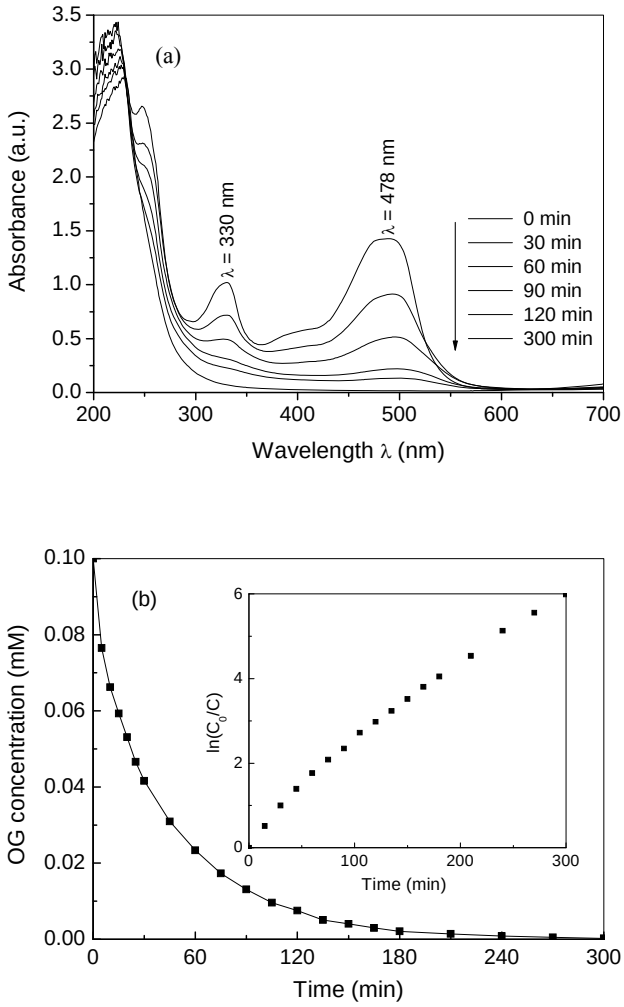

Fig. 10. Variation of the (a) OG absorption spectrum and (b) OG concentration during the photo-assisted electro-Fenton reaction using RVC as cathode, Pt as anode and Fe^{2+} as the externally dosing reagent under UV light irradiation.

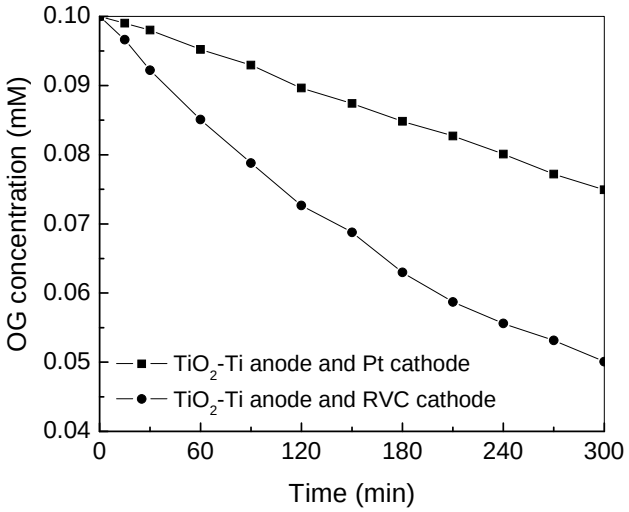

Fig. 11. Decrease of the OG concentration during the photoelectrocatalytic degradation reaction using a TiO_2-Ti mesh as anode and RVC (or Pt) as cathode under UV light irradiation.

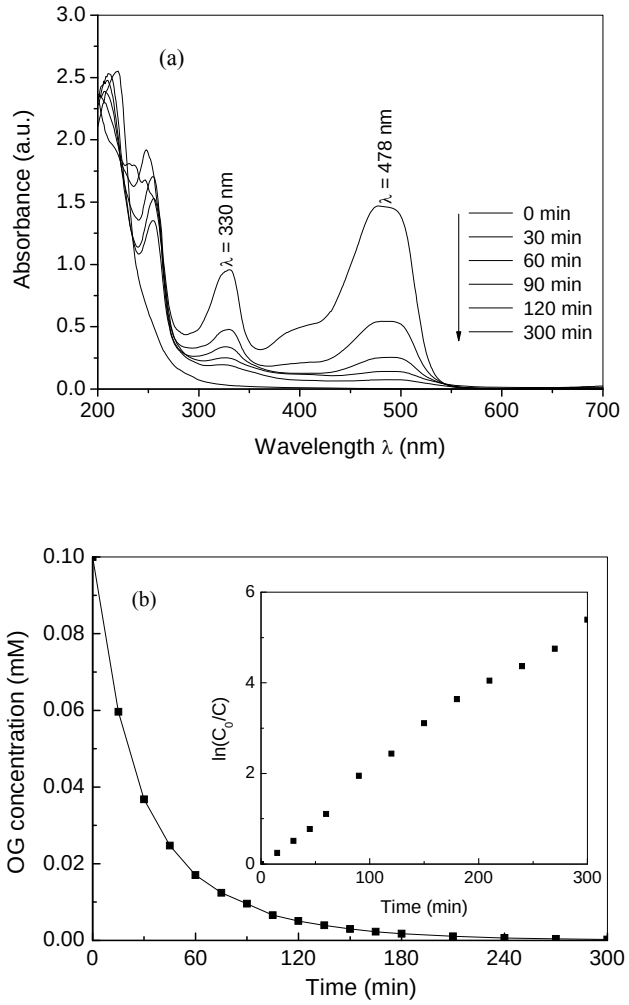

Fig. 12. Variation of the (a) OG absorption spectrum and (b) OG concentration during electro-Fenton photoelectrocatalytic oxidation reaction using RVC as cathode, TiO_2-Ti mesh as anode and Fe^{2+} as the dosing reagent under UV light irradiation.

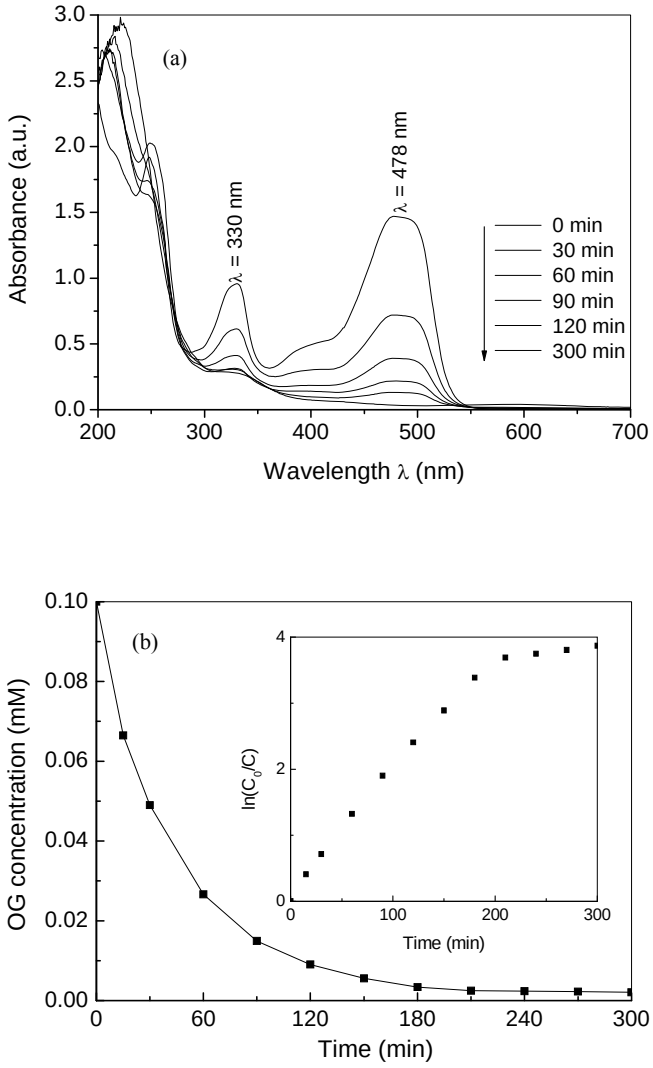

Fig. 13. Variation of the (a) OG absorption spectrum and (b) OG concentration during electro-Fenton photocatalytic oxidation reaction using RVC as cathode and Fe electrode with TiO_2 coating film as anode under UV light irradiation.

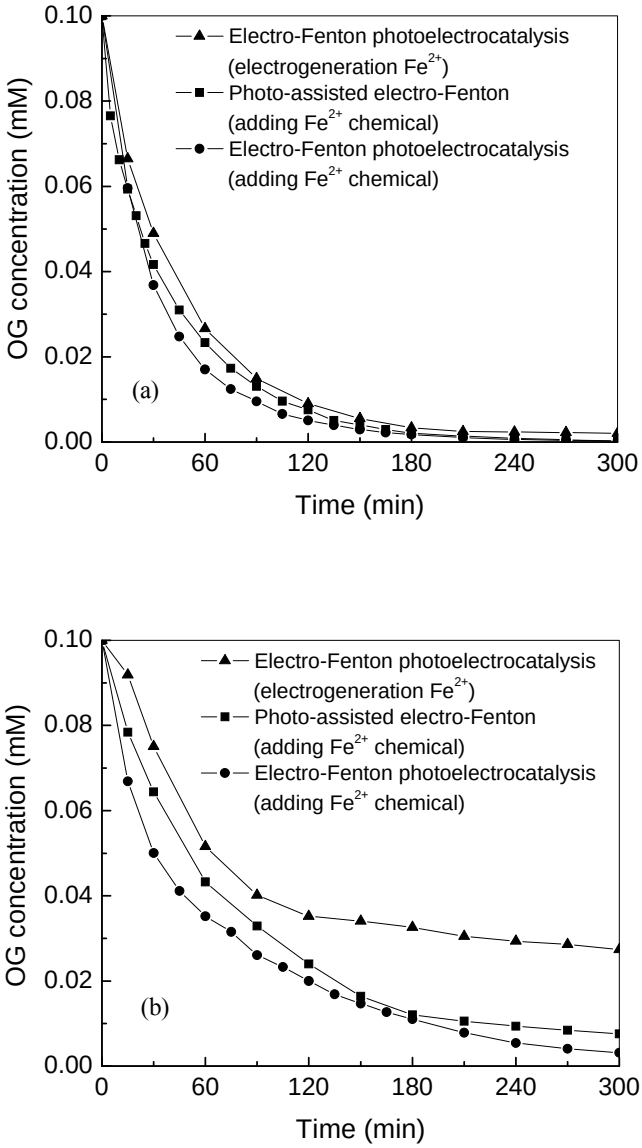

Fig. 14. Degradation of the OG dye at (a) λ = 478 nm and (b) λ = 330 nm during different photo-electro-assisted advanced oxidation processes.

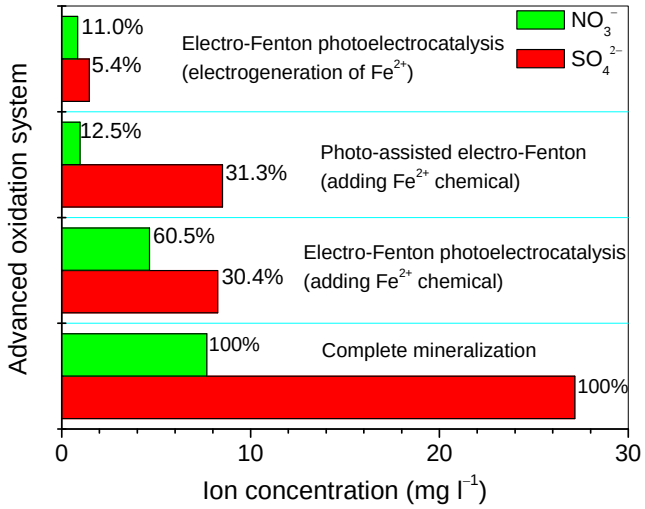

Fig. 15. Mineralization of OG in the photo-electro-assisted advanced oxidation systems.